Research Article | Vol. 29, No. 3 / 1 February 2021 / Optics Express 3543
Optics EXPRESS

All-optical high-speed modulation of THz transmission through silicon core optical fibers

TRYGVE SØRGÅRD,[1] THOMAS HAWKINS,[2] JOHN BALLATO,[2] ULF L. ÖSTERBERG,[3,4] AND URSULA J. GIBSON[1,3,*]

[1]Department of Physics, Norwegian University of Science and Technology, Trondheim NO- 7491, Norway
[2]Department of Materials Science and Engineering, Clemson University, Clemson SC 29634, USA
[3]Department of Applied Physics, Royal Institute of Technology, KTH, 10691 Stockholm, Sweden
[4]Thayer School of Engineering, Dartmouth College, Hanover, NH 03755, USA
[*]ursula.gibson@ntnu.no

Abstract: High speed optical modulation of THz radiation is of interest for information processing and communications applications. In this paper infrared femtosecond pulses are used to generate free carriers that reduce the THz transmission of silicon based waveguides over a broad spectral range. Up to 96% modulation is observed from 0.5 to 7 THz in an optical fiber with a 210 µm diameter gold-doped silicon core. The observed carrier recombination time of 2.0 ± 0.2 ns makes this material suitable for high speed all-optical signal processing. These results show both enhanced modulation depth and reduced carrier lifetime when compared to the performance of a high resistivity float zone silicon rectangular guide with comparable cross sectional area.

1. Introduction

Active components for the THz region of the electromagnetic spectrum are needed to bridge GHz and THz technology, e.g. next generation (beyond 5G) cellular networks, and short distance radar applications such as driverless cars [1]. Many applications require a modulator [2], preferably in a configuration that can be integrated with the THz source or transmission fiber. Optimal modulation would be fast, broadband, and deep, with a high native transparency. These requirements favor optically driven non-resonant solutions, and have resulted in extensive exploration of materials-based modulators, primarily semiconductors.

THz modulators based on semiconductors rely on fast temporal changes of free-carrier density, with deep modulation of THz beams successfully demonstrated in a variety of configurations [3–9]. Optical modulators are generally faster [10] and have greater modulation depth [11,12] than electrically controlled alternatives. For optical modulation, free carriers are excited within the material using a laser with photon energy higher than the bandgap ($E>E_g$), and the generated carriers reduce transmission of a signal beam with photon energies below the bandgap. The enhanced absorption coefficient induced by the excited free carriers follows the Drude model [13,14].

Fast modulation devices include reflection off a graphene layer on SU-8 resist [15] (358 GHz), GaAs defects in photonic crystals [16] (10 GHz) and InSb gratings on Si-GaAs substrates [17] (1.2 GHz). However, these structures show only $\approx 40-50\%$ modulation depth over a narrow bandwidth (tunable in the case of [17]). It has been shown that the modulation depth in a semiconductor can be increased by coating it with, e.g., graphene [4,5] or YAG-Ce [18]. The YAG-Ce coating also improved the modulation speed, but only to 4 MHz.

In addition, most THz modulators have been demonstrated in free-space systems [3–9,11,16] requiring a low-humidity environment to minimize absorption of the THz signal by water vapor. An integrated solution would increase the utility of this class of devices, as the modulator would be environmentally robust. The optimal material for a confined beam device would have high

#414545 https://doi.org/10.1364/OE.414545
Journal © 2021 Received 9 Nov 2020; revised 26 Dec 2020; accepted 11 Jan 2021; published 21 Jan 2021

Optics EXPRESS

baseline transmission, low dispersion and a short carrier lifetime. The semiconductor material shown to have optimal transmission is high-resistivity float zone (HRFZ) Si, however, this material is not ideal for modulation. While the measured lifetime in an undoped direct bandgap semiconductor such as GaAs is on the order of nanoseconds, it is up to several hundreds of microseconds in indirect bandgap semiconductors such as crystalline Si [19], where Shockley-Read-Hall recombination dominates. The modulation speed implication was confirmed in experiments with a parallel plate copper waveguide filled with high-resistivity float zone (HRFZ) Si, where 60% THz modulation was demonstrated [20], but THz transmission losses of the guide were high and operating frequencies were low, limited by the carrier recombination time [10].

Early work on THz modulation characterized both GaAs and pure silicon, and suggested that amorphous Si and Au-doped Si (Au:Si) might be appropriate for faster switching times [21]. However, short carrier lifetime is not the sole property needed; low dispersion and absorption are also critical for a possible integrated solution.

Carrier lifetimes in GaAs and amorphous Si are in the range of 1 ns [22, 23] and 80 ns [21], respectively. By implanting gold into crystalline Si, the carrier lifetime can be reduced to a few ns [22]. Although GaAs has the shortest lifetime and may thus feature faster modulation, it also has higher absorption [18] and a higher, more dispersive refractive index [19] than crystalline Si. Amorphous Si also has a higher refractive index than crystalline Si [21], and thus causes more dispersion for a fiber [21] of the same size. Furthermore, it has the longest carrier lifetime. Crystalline Si exhibits low loss and extremely low dispersion in the THz regime [20], and short carrier lifetimes can be induced by the addition of gold dopants. It is therefore the most promising material for an encapsulated/fiber modulator.

In this work, many of the favorable properties of semiconductor core optical fibers for active signal modulation, mentioned above, are used in a proof-of-concept active device. We report optical modulation of signals between 0.5 and 7 THz propagating in a Au:Si fiber. The fiber transmits high power in the unexcited state and demonstrates deep THz modulation with GHz speeds.

2. Experimental procedure

Terahertz spectroscopy provides a valuable way to assess the performance of various modulation schemes, and much has been published on the experimental methods; on air-plasma THz generation [23], THz detection in electro-optic crystals such as gallium phosphide (GaP) [24], time resolved THz spectroscopy [25] and optical pump THz probe spectroscopy [26].

In this study, two samples were used, a silica clad fiber drawn with the molten core method and a rectangular guide fabricated from a silicon wafer to yield a rectangular cross section waveguide [27]. The waveguide geometries were determined by the fabrication methods; the form of the waveguide does not affect the modulation properties. The cylindrical geometry of the fiber is due to the drawing process, where surface tension of the glass dominates the structural form; introduction of gold in the liquid silicon (and subsequent removal) assured a uniform distribution of dopant throughout the core. This procedure also recrystallized the core, yielding a sample of high structural quality. Compared to float zone production, fiber drawing typically reduces the purity of the core; to assure material properties comparable to the literature, a rectangular guide made by precision-sawing of a HRFZ wafer was used as a reference. The silicon portion of each had similar dimensions to minimize differences based on geometry. The Au:Si fiber was 9.6 mm long and had a core diameter of 210 μm. The HRFZ Si sample had core dimensions 125x290 μm, a length of 13 mm, and was sandwiched between two fused silica glass plates. The samples had approximately the same end-face area, and were polished using the same technique, so illumination by the excitation beam and surface recombination effects should be comparable.

Figure 1 shows the experimental THz setup [28]. The time-domain system is based on a Ti:Sapphire laser (Spectra-Physics, Solstice) where the main output has a central wavelength of

Optics EXPRESS

798 nm, pulse length of ~ 100 fs, 1 kHz rep rate and an average power of 3.2 W. Beams derived from this output are shown as dashed red lines in the figure. A beam splitter divides the output into a pump and probe beam, with approximately 90% of the power going to the THz pump. The pump beam (thick red dashes) is chopped at 200 Hz and passes through a BBO crystal, generating a second harmonic (thick blue dashes). The fundamental and its second harmonic are focused to a point and create an air-plasma that generates the THz pulse (light blue) with frequencies from 0.5 to 7 THz [29,30]. The THz radiation is collimated and directed using off-axis parabolic mirrors with focal lengths of 50.8 mm, while the pump beam and its harmonic are filtered out with a spectral splitter. Simulations of the waveguide transmission spectrum yield an approximate THz beam width of 1 cm, based comparison with experimental data. The THz pulses are coupled into and out of the waveguide using TPX lenses with focal lengths of 10 mm and diameters of 2 cm. The probe beam (intermediate red dashes) passes through a variable delay stage and is used to detect the THz signal via electro-optic detection by co-propagation through a 300 µm thick GaP crystal [31]. The probe delay stage (IMS-LM, Newport) is mechanically driven and moves 2 – 3 mm to measure the entire THz pulse length (up to ~ 6 picoseconds when dispersed). The IR probe beam continues on to a balanced photodetector (Zomega) connected to a lock-in amplifier (SR830, Stanford Research Systems) which drives the chopper. The THz beam path was encased in a plexiglass box containing calcium sulfate (VWR Drierite) to keep the relative humidity below 5% at room temperature. A series of IR windows (marked in gray along the box edge) were mounted in the walls to maximize the IR power inside the controlled atmosphere.

To modulate transmission, a third beam, designated as the excitation beam (EB) was used to excite free carriers in the sample, as illustrated in Fig. 2. In this work, two different excitation sources were used to generate carriers (marked EB1 and EB2 in Fig. 1). These beams were incident on the end of the fiber at an angle of ~ 15° due to geometrical constraints imposed by the sample holder. A lens of focal length 30 cm was used to focus EB1, and one with a focal length of 10 cm was used with EB2. The exit end of the fiber was illuminated; a CMOS camera image of the illuminated end of the Au:Si fiber is shown an inset in Figure 1. The specifications of these two beams are summarized in Table 1. The absorption depth is reported to be 10 µm [32], with no excess infrared absorption expected at the power levels employed [33].

Table 1. Specifications of the two excitation beams used in the experiments. Each had a central wavelength of 798 nm.

Excitation beam	EB1	EB2
Pulse width [fs]	100	275
Repetition rate [Hz]	82 M	1 k
Power [mW]	300	0.8
Pulse energy [nJ]	3.67	800
#Photons/pulse	1.5e10	3.2e12

EB1 is a 100 fs pulsed laser beam with a repetition rate of 82 MHz and central wavelength of 798 nm (solid red line), which is a secondary output of the Ti:sapphire laser. While this repetition rate is high enough to be considered continuous wave for the ~ ms recombination lifetime HRFZ material [4], for the gold-doped material this is not the case. The laser, when started, has a variable offset of up to 2 ns between the MHz pulses and the amplified output derived from them. The offset is fixed and stable after startup. The timing affects the modulation depth, and the data shown is from those runs where the deepest modulation was observed, implying a small offset between the MHz excitation and THz pulses. For short recombination lifetimes, the fixed time delay between the THz and excitation pulses allows measurement of relative modulation. The modulation depth as a function of carrier injection level was studied by modifying the excitation power with a neutral density filter.

Optics EXPRESS

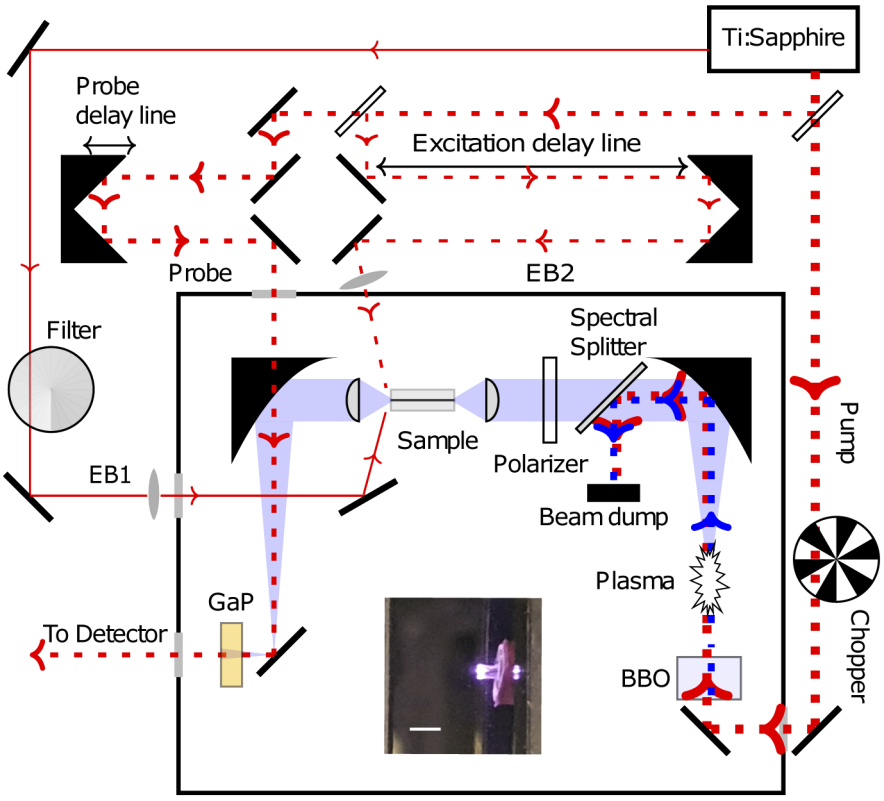

Fig. 1. Schematic of the experimental setup. The Ti:sapphire (MaiTai) laser delivers 100 fs modelocked (ML) pulses with a repetition rate of 82 MHz (EB1, thin red line). 60% of the MaiTai power is amplified, reducing the repetition rate to 1kHz (red dashed lines). The amplified pulses are split into pump (THz generation) and probe (THz detection) beams. Carriers were generated by either the ML pulses (EB1) or a fraction of the probe beam from the amplified pulses (EB2). The arrival time of the EB2 excitation pulses could be varied over several nanoseconds with reference to the THz pulses, employing a 0.5 m delay line. Inset is a CMOS camera image of the illuminated fiber end (scale bar 2 mm).

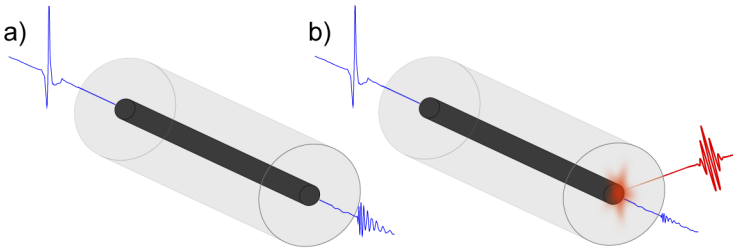

Fig. 2. Fiber geometry for a) unmodulated case in which the THz pulse is focused into and travels through the silicon waveguide, and b) modulated case where the IR pulse is focused on the output end of the fiber, illuminating the semiconductor core.

Optics EXPRESS

The alternate excitation, EB2 (thin red dashes in Fig. 1) is derived from the probe beam, and is therefore synchronized with the THz pump and probe beams with the same 1 kHz repetition rate. This beam passed through a delay stage so that the arrival time at the sample could be varied relative to the THz pulse. The delay stage consisted of a retro-reflector on a rail which was moved over a range of 0.5 m to allow estimation of the carrier recombination time. EB2 passed directly through the plexiglass box to simplify the geometry, and this stretched the pulse duration from ~ 100 to ~ 275 fs. Measurements were performed by taking a full time-sweep over the probe delay line with the EB2 delay line in a fixed position. The EB2 path length was then increased by a 6 cm increment, corresponding to 0.2 nanoseconds, before doing a new probe sweep. Ten scans were collected at each position of the retro-reflector. Comparison of modulation depths from the kHz and MHz excitation beams were within the uncertainty introduced by differences in absorption and beam alignment.

3. Results & discussion

Two sets of experiments were undertaken, first with EB1 to examine the modulation depth power dependence, and a second set, with EB2, to characterize the recombination time, and hence the modulation frequency limit.

Modulation depth is defined as

$$M(\omega) = \left| \frac{E_0(\omega) - E_M(\omega)}{E_0(\omega)} \right|, \tag{1}$$

where E_0 is the transmitted field amplitude without illumination and E_M is the modulated signal. By changing the power of EB1 using the variable neutral density filter, the power-dependent modulation depth of the two samples were measured. The top two panels of Fig. 3 show the modulation depth at different pump powers for the Au:Si and the HRFZ Si. Fig. 3(a) shows $\geq$ 70% modulation from 1 – 6 THz, with a maximum of 96% for the Au:Si fiber. The HRFZ Si sample (Fig. 3(b)) displays significantly shallower modulation, particularly for higher frequencies. The shape of the spectrum in Fig. 3(b) is due to features seen in transmission measurements, as reported by Gingras [34] for asymmetric guides and for the rectangular guide used here as a function of exact coupling conditions [27]. These features are broadened during the modulation experiments, leading to the stepped appearance seen in the figure. As the features are coupling dependent, they are taken to be system and sample related, rather than fundamental. The power-dependence of the modulation depth for selected frequencies is shown in Fig. 3(c) for the Au:Si fiber and Fig. 3(d) for the HRFZ waveguide. The low frequency curves show saturation at high power. However, the high-frequency modulation was still increasing at the power available, suggesting that improved modulation depth for these frequencies can be achieved with higher excitation power or improved illumination geometry. The reduced modulation depth for the HRFZ Si is likely related to the diffusion of carriers through the sample, given the long recombination time. The difference in performance suggests that the steep gradient in carrier concentration for the Au:Si may be important for the modulation.

The carrier recombination time was measured by varying the optical path length of EB2, the pulses of which are synchronized with the THz signal. Both the time traces and maximum amplitude of the THz pulses were recorded as a function of delay time. Fig. 4(a) and Fig. 4(b) show time-traces of the THz transmission through the fiber and the rectangular waveguide with EB2 pulses arriving at different times with respect to the THz signal. The Au:Si data shows recovery of the signal amplitude as the arrival times of the excitation and THz pulses separate, indicating that carriers absorbing the signal have a short lifetime compared to those in the HRFZ sample. Figure 4(c) shows the peak signal strength as a function of delay time. The data was fit

Optics EXPRESS

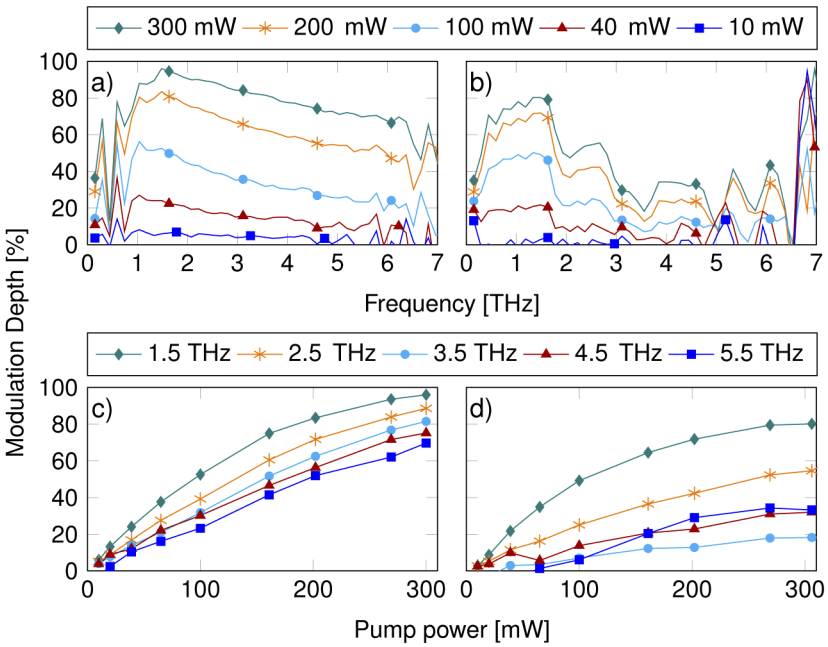

Fig. 3. Power-dependent modulation results. a-b) show modulation depth as a function of frequency for different excitation pulse energies for the Au:Si fiber and the HRFZ Si rectangular waveguide. c-d) show the corresponding modulation depth as a function of pump power for selected frequencies for each sample.

to an exponential recovery function

$$T(t) = 1 - \Theta(t) T_0 e^{-t/\tau}, \tag{2}$$

where $T(t)$ is the relative transmission at time t after the excitation pulse arrives, and $\Theta(t)$ is the Heaviside step function. T_0 and τ are fitted parameters and represent the reduced transmission immediately after the excitation beam arrives, and the carrier lifetime, respectively. The error bars come from the standard deviation of relative peak power for the ten measurements performed at each delay line length. The parameter values for exponential fit for the Au:Si fiber in Fig. 4 are $T_0 = 0.86 \pm 0.05$ and $\tau = 2.0 \pm 0.2$ ns. For the rectangular waveguide, there is lower signal than the reference at "negative time", i.e. when EB2 arrives at the sample after the THz pulse has already passed through. This means that the sample still holds carriers generated from the previous pulse, implying a lifetime on the order of ms.

The change in optical properties by excited free carriers in a semiconductor is most commonly described by the Drude dispersion model for metals [13,14].

$$\varepsilon(\omega) = \varepsilon_\infty - \frac{\omega_p^2}{-\omega^2 + i\omega/\tau}, \tag{3}$$

where $\varepsilon(\omega)$ and $\varepsilon(\infty)$ are the relative permittivities at frequency ω and at $\omega \to \infty$, respectively. ω_p is the plasma frequency and τ is the carrier relaxation time. The plasma frequency is

$$\omega_p = \sqrt{\frac{n_e e^2}{\varepsilon_0 m^*}} \tag{4}$$

where n_e is the electron density, e is the electron charge, ε_0 is the permittivity of free space, and m^* is the effective carrier mass ($0.26 m_0$ [20]). Since it is related to the number of free-carriers, it

Optics EXPRESS

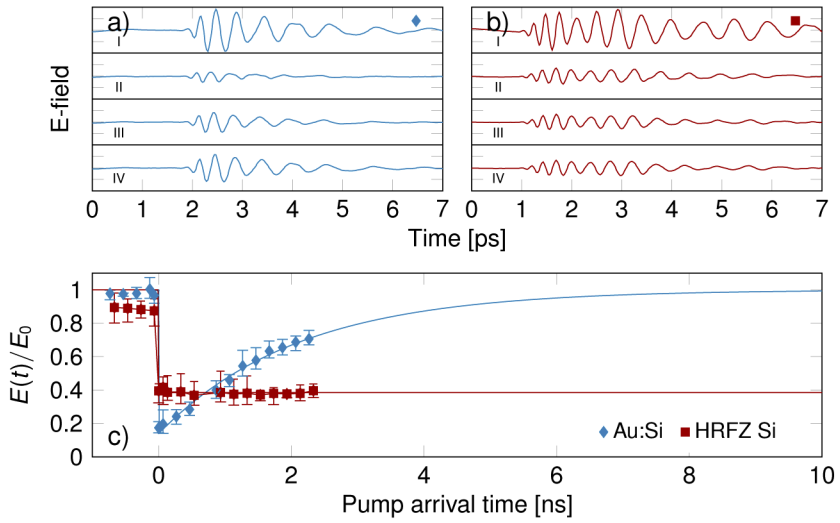

Fig. 4. Modulation with EB2 pulses a) Time-domain signals from the Au:Si fiber. b) Time-domain signals from the HRFZ Si waveguide [curves: I) reference signal, no modulation and II) 0 ns III) 1.1 ns IV) 2.3 ns delay.] Each division on the y-axis corresponds to a signal strength of 50 µV. c) Relative signal strength of the time-domain signals as a function of delay. E_0 is the peak signal strengths of the un-modulated signal, and $E(t)$ is the signal when the modulation beam arrives at time t relative to the THz signal.

is dependent on both the doping level of the material and the energy of the excitation beam. The change in optical parameters due to the optical modulation can be expressed as [20]

$$\frac{E_M(\omega)}{E_0(\omega)} = |1 - M|e^{-i\phi} = e^{-\alpha_M(\omega)d/2}e^{-i(n_M(\omega)-n_0)\omega d/c} \tag{5}$$

where d is the depth of material containing additional free carriers and depends on the absorption of the excitation beam and on the diffusion length of carriers in the material, and M is the modulation depth. This leads to the expressions

$$\alpha_M(\omega) = -\frac{2}{d}\ln|1 - M| \tag{6}$$

$$n_M(\omega) = n_0(\omega) + \frac{\phi(\omega)c}{d\omega} \tag{7}$$

which can be fit to Drude model (Eq. (3)).This is the simplest model of the optical response, and while rigorous treatment of the details of the fitting procedure have been reported [35], and improvements to the model can be made by distinguishing the relaxation between inter- and intravalley scattering [13] or by adding energy-dependence to the carrier-relaxation rate [14] or spatially varying carrier concentration, suppression of THz transmission can be adequately modelled based on induced free carrier absorption.

Figure 5 shows a comparison between the measured refractive index and absorption for the Au-Si fiber and a least-squares fit of the Drude model. Panel a) shows the relation between the Drude absorption and the modulation depth

$$M(\omega) = 1 - e^{-\alpha_M(\omega)d/2}. \tag{8}$$

The model assumes that there is a constant density of carriers in a slab at the end of the fiber; while the value used (d=25 µm) is somewhat larger than the absorption depth of the IR photons, it

Optics EXPRESS

gives improved high frequency fits with a minimum number of adjustable parameters. The small changes in refractive index over this short distance are expected to have little influence on the modulation. The left side of Table 2 shows the estimated carrier density and plasma frequency calculated from the pulse energy of EB1 at 100 – 300 mW within a volume $d\pi a^2$, where a is the fiber core radius (105 µm). The right side of the table shows the parameters used to obtain the fits in Fig. 5. The absorption varies with pump power as expected and the values used for the fit are within an order of magnitude of the values based on the measured input energy of the pulses. The geometry used, with carrier excitation at the end of the fiber, represents a hybrid between prior techniques - as it propagates, the THz wave will be exposed to an increasing density of carriers, similar to the profile of the waveguide excitation used by Cooke [20]. At the exit face of the fiber, the abrupt change of the material properties will induce reflection, as seen with photoexcited switches [36]. In addition, the carrier density induced by the side-illuminating beam is expected to be asymmetric, disrupting established modes within the fiber. While it is beyond the scope of this initial report to pursue these effects in detail, there are rich phenomena to be explored in these fibers and in planar samples made with this material.

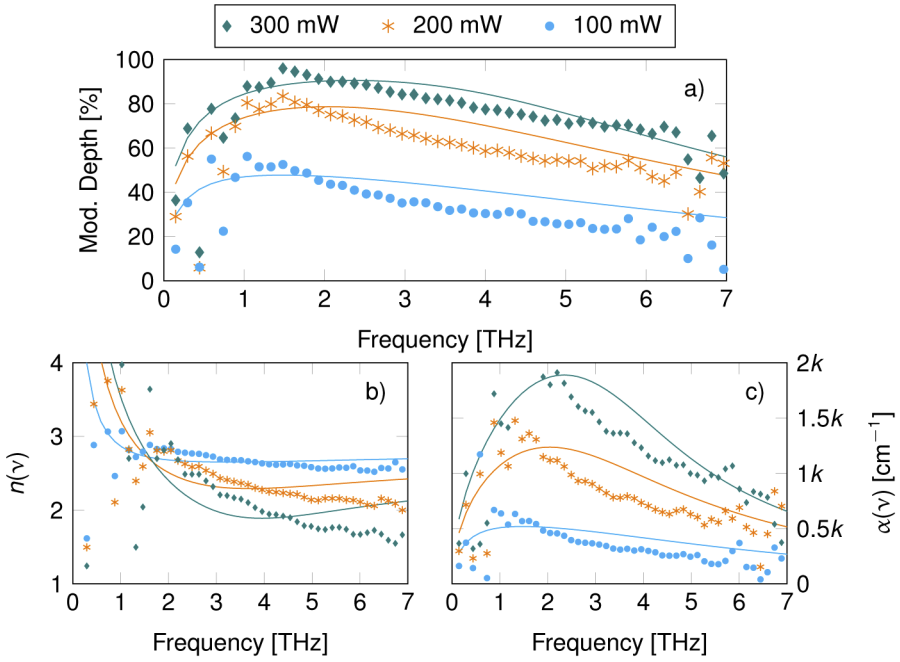

Fig. 5. Drude model fits to changes induced in a) modulation depth, b) refractive index and c) absorption by MaiTai in Au-Si fiber, assuming 100% photon conversion

Table 2. Left: Carrier density and plasma frequency calculated from the measured power of EB1. Right: Fitting parameters of the curves in Fig. 5. Both sides use d = 25 µm

Power [mW]	n_e [cm^{-3}]	$\omega_p/2\pi$ [THz]	ε_∞	τ [ps]	$\omega_p/2\pi$ [THz]
100	0.56e16	1.32	7.77	0.023	6.96
200	1.14e16	1.88	7.01	0.031	9.36
300	1.70e16	2.30	6.11	0.039	10.37

Optics EXPRESS

4. Conclusion

We have demonstrated high-speed all-optical modulation of broadband THz signals within a silicon core optical fiber with low levels of gold dopants. The potential for active as well as passive [27] functions and the possibilities for deployment in 2-d circuits make a strong case for further investigation of this material system for THz signal management. The low loss properties of Au:Si combined with high modulation speed make it preferable to GaAs, crystalline Si and amorphous Si.

Data on silicon waveguides with and without gold show that the dopants dominate carrier lifetimes, and the Au:Si data indicate the possibility of GHz signal modulation over a wide THz frequency range, vastly outperforming HRFZ Si. In addition, the Au:Si fiber showed increased modulation depth over HRFZ at high frequencies. Deeper penetration of longer excitation wavelengths would permit perpendicular illumination of a fiber to modulate the signal without any exposure of the THz to the ambient, removing humidity-induced limitations. The small size of the device demonstrated here offers new possibilities for THz signal manipulation beyond free-space applications, and implantation and annealing of silicon wafers would allow utilization of this material for integrated photonic, free-space and pixelated modulation schemes.

Funding. Norges Forskningsråd (262232, 262644); Norges Teknisk-Naturvitenskapelige Universitet; J. E. Sirrine Foundation.

Acknowledgments. The authors would like to thank Hogne Lysne, Kjell Martin Mølster and Seunghan Song for fruitful discussions. We would also like to thank Cristine Kores and Prof. Fredrik Laurell at the Royal Institute of Technology, KTH, Sweden, for the HRFZ Si sample.

Disclosures. The authors declare no conflicts of interest.

References

1. H. Aghasi, S. M. H. Naghavi, M. Tavakoli Taba, M. A. Aseeri, A. Cathelin, and E. Afshari, "Terahertz electronics: Application of wave propagation and nonlinear processes," Appl. Phys. Rev. **7**(2), 021302 (2020).
2. K. J. Kaltenecker, E. J. R. Kelleher, B. Zhou, and P. U. Jepsen, "Attenuation of thz beams: A "how to" tutorial," J. Infrared, Millimeter, Terahertz Waves **40**(8), 878–904 (2019).
3. M. Liu, X. Yin, E. Ulin-Avila, B. Geng, T. Zentgraf, L. Ju, F. Wang, and X. Zhang, "A graphene-based broadband optical modulator," Nature **474**(7349), 64–67 (2011).
4. P. Weis, J. L. Garcia-Pomar, M. Höh, B. Reinhard, A. Brodyanski, and M. Rahm, "Spectrally wide-band terahertz wave modulator based on optically tuned graphene," ACS Nano **6**(10), 9118–9124 (2012).
5. Q.-Y. Wen, W. Tian, Q. Mao, Z. Chen, W.-W. Liu, Q.-H. Yang, M. Sanderson, and H.-W. Zhang, "Graphene based all-optical spatial terahertz modulator," Sci. Rep. **4**(1), 7409 (2015).
6. H. K. Yoo, Y. Yoon, K. Lee, C. Kang, C.-S. Kee, I.-W. Hwang, and J. W. Lee, "Highly efficient terahertz wave modulators by photo-excitation of organics/silicon bilayers," Appl. Phys. Lett. **105**(1), 011115 (2014).
7. T. He, B. Zhang, J. Shen, M. Zang, T. Chen, Y. Hu, and Y. Hou, "High-efficiency thz modulator based on phthalocyanine-compound organic films," Appl. Phys. Lett. **106**(5), 053303 (2015).
8. Z.-W. Shi, X.-X. Cao, Q.-Y. Wen, T.-L. Wen, Q.-H. Yang, Z. Chen, W.-S. Shi, and H.-W. Zhang, "Terahertz modulators based on silicon nanotip array," Adv. Opt. Mater. **6**(2), 1700620 (2018).
9. L. Cong, Y. K. Srivastava, H. Zhang, X. Zhang, J. Han, and R. Singh, "All-optical active thz metasurfaces for ultrafast polarization switching and dynamic beam splitting," Light: Sci. Appl. **7**(1), 28 (2018).
10. Z. T. Ma, Z. X. Geng, Z. Y. Fan, J. Liu, and H. D. Chen, "Modulators for terahertz communication: The current state of the art," Research **2019**, 1–22 (2019).
11. Z. Xie, X. Wang, J. Ye, S. Feng, W. Sun, T. Akalin, and Y. Zhang, "Spatial terahertz modulator," Sci. Rep. **3**(1), 3347 (2013).
12. W. Chan, H.-T. Chen, A. Taylor, I. Brener, M. Cich, and D. Mittleman, "A spatial light modulator for terahertz beams," Appl. Phys. Lett. **94**(21), 213511 (2009).
13. M. van Exter and D. Grischkowsky, "Optical and electronic properties of doped silicon from 0.1 to 2 thz," Appl. Phys. Lett. **56**(17), 1694–1696 (1990).
14. M. van Exter and D. Grischkowsky, "Carrier dynamics of electrons and holes in moderately doped silicon," Phys. Rev. B **41**(17), 12140–12149 (1990).
15. A. C. Tasolamprou, A. D. Koulouklidis, C. Daskalaki, C. P. Mavidis, G. Kenanakis, G. Deligeorgis, Z. Viskadourakis, P. Kuzhir, S. Tzortzakis, M. Kafesaki, E. N. Economou, and C. M. Soukoulis, "Experimental demonstration of ultrafast thz modulation in a graphene-based thin film absorber through negative photoinduced conductivity," ACS Photonics **6**(3), 720–727 (2019).

Optics EXPRESS

16. L. Fekete, F. Kadlec, P. Kužel, and H. Němec, "Ultrafast opto-terahertz photonic crystal modulator," Opt. Lett. **32**(6), 680–682 (2007).
17. L. Deng, J. Teng, H. Liu, Q. Y. Wu, J. Tang, X. Zhang, S. A. Maier, K. P. Lim, C. Y. Ngo, S. F. Yoon, and S. J. Chua, "Direct optical tuning of the terahertz plasmonic response of insb subwavelength gratings," Adv. Opt. Mater. **1**(2), 128–132 (2013).
18. J. Li and M. Hu, "Enhancement of silicon modulating properties in the thz range by yag-ce coating," Sci. Rep. **10**(1), 6605 (2020).
19. T. Nozokido, H. Minamide, and K. Mizuno, "Modulation of submillimeter wave radiation by laser-produced free carriers in semiconductors," Electron. Comm. Jpn. Pt. II **80**(6), 1–9 (1997).
20. D. G. Cooke and P. U. Jepsen, "Optical modulation of terahertz pulses in a parallel plate waveguide," Opt. Express **16**(19), 15123–15129 (2008).
21. H. Salzmann, T. Vogel, and G. Dodel, "Subnanosecond optical switching of far infrared radiation," Opt. Commun. **47**(5), 340–342 (1983).
22. C. Hu, *Modern Semiconductor Devices for Integrated Circuits* (Prentice Hall, 2010).
23. I.-C. Ho and X.-C. Zhang, "Application of broadband terahertz spectroscopy in semiconductor nonlinear dynamics," Front. Optoelectron. **7**(2), 220–242 (2014).
24. Y. Cai, I. Brener, J. Lopata, J. Wynn, L. Pfeiffer, J. B. Stark, Q. Wu, X. C. Zhang, and J. F. Federici, "Coherent terahertz radiation detection: Direct comparison between free-space electro-optic sampling and antenna detection," Appl. Phys. Lett. **73**(4), 444–446 (1998).
25. K. Iwaszczuk, D. G. Cooke, M. Fujiwara, H. Hashimoto, and P. U. Jepsen, "Simultaneous reference and differential waveform acquisition in time-resolved terahertz spectroscopy," Opt. Express **17**(24), 21969–21976 (2009).
26. M. Monti, S. X. Tao, M. Staniforth, A. Crocker, E. Griffin, A. Wijesekara, R. A. Hatton, and J. Lloyd-Hughes, "Efficient intraband hot carrier relaxation in the perovskite semiconductor cs1-xrbxsni3 mediated by strong electron-phonon coupling," J. Phys. Chem. C **122**(36), 20669–20675 (2018).
27. T. Sørgård, S. Song, P. E. Vullum, C. Kores, K. M. Mølster, F. Laurell, T. Hawkins, J. Ballato, U. L. Österberg, and U. J. Gibson, "Broadband infrared and thz transmitting silicon core optical fiber," Opt. Mater. Express **10**(10), 2491–2499 (2020).
28. K. M. Mølster, T. Sørgård, H. Laurell, C. Canalias, V. Pasiskevicius, F. Laurell, and U. Österberg, "Time-domain spectroscopy of $KTiOPO_4$ in the frequency range 0.6-7.0 THz," OSA Continuum **2**(12), 3521–3538 (2019).
29. D. J. Cook and R. M. Hochstrasser, "Intense terahertz pulses by four-wave rectification in air," Opt. Lett. **25**(16), 1210–1212 (2000).
30. X. Xie, J. Dai, and X.-C. Zhang, "Coherent control of thz wave generation in ambient air," Phys. Rev. Lett. **96**(7), 075005 (2006).
31. Q. Wu and X.-C. Zhang, "7 terahertz broadband gap electro-optic sensor," Appl. Phys. Lett. **70**(14), 1784–1786 (1997).
32. M. A. Green and M. J. Keevers, "Optical properties of intrinsic silicon at 300 k," Prog. Photovoltaics **3**(3), 189–192 (1995).
33. R. Aharoni, M. Sinvani, Y. R. Tischler, and Z. Zalevsky, "Basic model of absorption depth and injection levels in silicon under intermediate illumination levels," Opt. Commun. **291**, 1–6 (2013).
34. L. Gingras, M. Georgin, and D. G. Cooke, "Optically induced mode coupling and interference in a terahertz parallel plate waveguide," Opt. Lett. **39**(7), 1807–1810 (2014).
35. H.-K. Nienhuys and V. Sundström, "Intrinsic complications in the analysis of optical-pump, terahertz probe experiments," Phys. Rev. B **71**(23), 235110 (2005).
36. F. A. Hegmann and M. S. Sherwin, "Generation of picosecond far-infrared pulses using laser-activated semiconductor reflection switches," in *Millimeter and Submillimeter Waves and Applications III*, vol. 2842 M. N. Afsar, ed., International Society for Optics and Photonics (SPIE, 1996), pp. 90–105.